Simulated GAIA observations of galaxies

Mattia Vaccari Erik Høg

27 August 1999 – SAG_CUO_69

Abstract

Simulated GAIA observations of galaxies, including flux maps obtained by their stacking, are presented. The simulations are obtained for the Astro-2 BBP and are based on HST WFPC2 data and on realistic assumptions about BBP performance with respect to electron count rate, PSF and noise. A comparison between the results obtained with the baseline sample size of 6×8 pixels and the three smaller sizes of 4×8, 6×4 and 4×4 pixels is carried out, and it is concluded that these latter choices, regardless of the higher readnoise per unit area, give both better resolution and more accurate photometry. It appears for instance that flux maps reconstructed from 50 observations carried out with 6×4 pixels/sample would have a resolution of about 350 mas. A simple preliminary aperture photometry in V of HII regions and median surface photometry of various sky zones in the background were carried out in order to characterize the observed sky area containing a part of the M100 galaxy.

1 Introduction

In SAG_CUO_61 (Vaccari and Høg 1999) it was shown by analytical methods that GAIA would be able to detect normal galaxies with a total I magnitude brighter than about 16.5 in the ASM1 and to measure surface brightness out to the half-light radius of these in the BBP. Subsequently, in SAG_CUO_66 (Vaccari, Høg and Makarov 1999) we presented a flux map obtained by stacking of 50 simulated BBP observations. In these reports, a sample size of 6×8 pixels/sample had been tentatively chosen, being the baseline for the observation of stars taking place in the Astro-2 BBP for most of the mission, but further optimization was desirable.

In this report the techniques used in simulating observations and in stacking them into a flux map are described, and a discussion of the results is given. Some refinements were made with respect to the program used to generate the flux map presented in SAG_CUO_66, leading to a more accurate simulation of GAIA performance. For the sake of comparison, simulations were carried out with the four sample sizes of 6×8, 4×8, 6×4 and 4×4 pixels, which allowed us to better understand how the sample size affects the resolution of the flux maps.

Section 2 specifies which HST data were used in the simulations, always a part of the bright Virgo cluster spiral galaxy M100. In Section 3 a comparison is made between the performance of HST WFPC2 and GAIA BBP. Sections 4 and 5 outline the techniques used in generating simulated observations and in stacking them into flux maps, respectively. Section 6 presents the flux maps and discusses some issues related to their reconstruction. In Section 7 an estimate of the photometric accuracy achievable by a simple aperture photometry is given by separately analysing the original HST data and the flux maps.

2 HST images

Our simulations were based on data obtained with the HST WFPC2. The instrument's field of view is divided into four cameras, each consisting of a 800×800 pixel CCD. The Planetary

Camera (PC) operates at an image scale of 45.5 mas/pixel, whereas the three Wide Field Cameras (WFCs) operates at 96.6 mas/pixel. The data were retrieved from the Hubble Data Archive (HDA) (`http://archive.stsci.edu`) of the Space Telescope Science Institute (STScI). Only the HDA calibrated data, i.e. the data processed through the socalled calibration pipeline carried out at the STScI, were used. These are affected by problems common to any astronomical instrument (e.g. limited throughput, not point-like PSF, cosmic ray hits and noise) as well as by the instrument's peculiar problems (described by Holtzman et al. 1995a and Biretta et al. 1996). We did not try to correct the calibrated data for any of these effects, thus assuming that they faithfully represented the "real sky". In particular, they were used without any cut at some noise level. In other words, in order to be conservative, the HST images were taken to be ideal. The reason for this simplified approach was that we were mainly interested in simulating how GAIA would reproduce a given sky image containing lots of subarcsec details. Note also that in Subsections 3.2 and 3.3 it is shown that the assumption of ideal HST images is essentially correct with respect to PSF and noise consideration.

3 GAIA vs HST

As a first step a comparison between HST on-orbit performance and GAIA specifications as they are presently foreseen was carried out. This comparison mainly focused on the instruments' electron count rate, point spread function and noise.

3.1 Electron count rate

The transformations from the WFPC2 flight system to the Landolt $UBVRI$ system obtained by Holtzman et al. 1995b (and therein given by Equation 8 with the coefficients of Table 7) allows one to convert HST data number counts into Landolt $UBVRI$ magnitudes, or to estimate HST electron count rates for a star of a given standard magnitude and colour. For a star of e.g. $V = 15$ and $V - I = 1$, an exposure with the F555W filter (the socalled HST V filter) gives an electron count rate of about 7300 e^- s^{-1}.

Estimates of GAIA electron count rate for different CCDs as a function of magnitude and spectral type of stars were provided by L. Lindegren in a private communication. According to these a star of $V = 15$ and spectral type G2V with an $A_V = 0$ has a colour index of $V - I = 0.72$ and gives an electron count rate of about 8400 e^- s^{-1} on CCD#1B.

Thus the electron count rate turns out to be almost the same (GAIA's is actually higher), notwithstanding the much bigger aperture of HST, but this can be explained by the seven reflections taking place in the HST OTA and WFPC2, and to a minor extent by the higher quantum efficiency of GAIA's CCDs. On this basis, in the simulations we assumed the same rate for the two instruments.

3.2 Point Spread Function

The PSF of the HST WFPC2 is accurately described by Holtzman et al. 1995a. In particular, Figure 5 therein shows that when observations with the broad-band, $UBVRI$-like WFPC2 filters are made the 50%-light diameter, i.e. the diameter of the circle enclosing 50% of the light coming from a point source, is about 80 and 130 mas, for the PC and the WFCs respectively.

The GAIA PSF modelling was based on SAG_LL_025 (Lindegren 1999a). An adaptation of L.Lindegren's syntpsf.f written by A.Brown was used to output the PSF as a fits file. In the calculations we assumed a colour index of $V - I = 1$ mag and used the corresponding s_k coefficients the aforementioned report gives in Table 1. Since only the astrometric field was therein considered in the wave-front error simulations, we calculated the PSF at the field point number 10, which is the nearest to the central region of the BBP. The four sample sizes of 6×8, 4×8, 6×4 and 4×4 pixels were separately considered, and in all cases a TDI interval equal to the sample size along scan was assumed. Then, in order to model the all-mission effective PSF, i.e. the PSF of an all-mission flux map, we generated a set of 50 randomly distributed scan directions, we accordingly rotated the one-scan PSF using the ROT IDL routine and summed up the rotated PSFs thus obtained.

The properties of the resulting PSFs are illustrated in Figures 1 and 2, showing the one-scan and 50-scan PSFs, respectively. The first plot of each row is a a contour plot of the two-dimensional PSF, with the brightest contour drawn at a surface brightness level 0.5 magnitudes fainter than the maximum and altogether seven contours drawn at intervals of one magnitude. In the second one, the encircled energy curve of the PSF is given, whereas in the third and fourth one the one-dimensional PSF profiles along the two axes are drawn.

For instance, one can see that in general a one-scan PSF is not exactly centred at the point (0,0), due to wave-front errors and that a 50-scan PSF is not perfectly circular, due to random fluctuations in the scan directions. Besides, in general the encircled energy curve does not depend significantly on the number of scans.

The 50%-light diameter d_{50} and the 90%-light diameter d_{90} (i.e. the diameters of the circles enclosing 50% and 90% of the energy, respectively) of the 50-scan PSFs are given by Table 1 together with the FWHM. It should be noted that d_{50} and d_{90} depend above all on the length of the sample major side and that d_{50} and the FWHM can be very different, the FWHM usually being smaller than d_{50}. It is seen that the difference increases with the PSF asymmetry, which in turn increases with the y/x ratio of the sample size. This was to be expected, since an asymmetric PSF has relatively wider wings. However, this effect is not particularly significant for the two smaller and more symmetric sample sizes of 6×4 and 4×4 pixels. It was also verified that with an even smaller and more symmetric sample of 6×2 pixels, i.e. a square sample, there is not a significant improvement in any of these three parameters.

Table 1: Values of d_{50}, d_{90} and FWHM. 50%-light diameter, 90%-light diameter and FWHM of GAIA 50-scan PSFs for different sample sizes.

	d_{50}	d_{90}	FWHM
6×8	520	940	400
4×8	500	920	280
6×4	340	640	345
4×4	300	640	265

The effective PSF of the flux map obtained by stacking of simulated observations will actually be slightly wider than given above, since the HST and GAIA PSFs both contribute to smear it. Taking this into account, the 50%-light diameter can be estimated by means of the quadratic formula $d_{50,sim} = \sqrt{d^2_{50,HST} + d^2_{50,GAIA}}$, which however gives values that do not differ much from those given in Table 1 for any combination of WFPC2 camera and BBP sample size.

Note that the PSFs thus obtained are sampled with a step of 1/4 pixel along both directions, and therefore need to be resampled and renormalized before convolution with GAIA observations (see Section 4).

3.3 Noise

Only photon noise and readnoise were introduced in GAIA observations, whereas possible contributions due to cosmic ray hits and non-optimal CCD performance were not included.

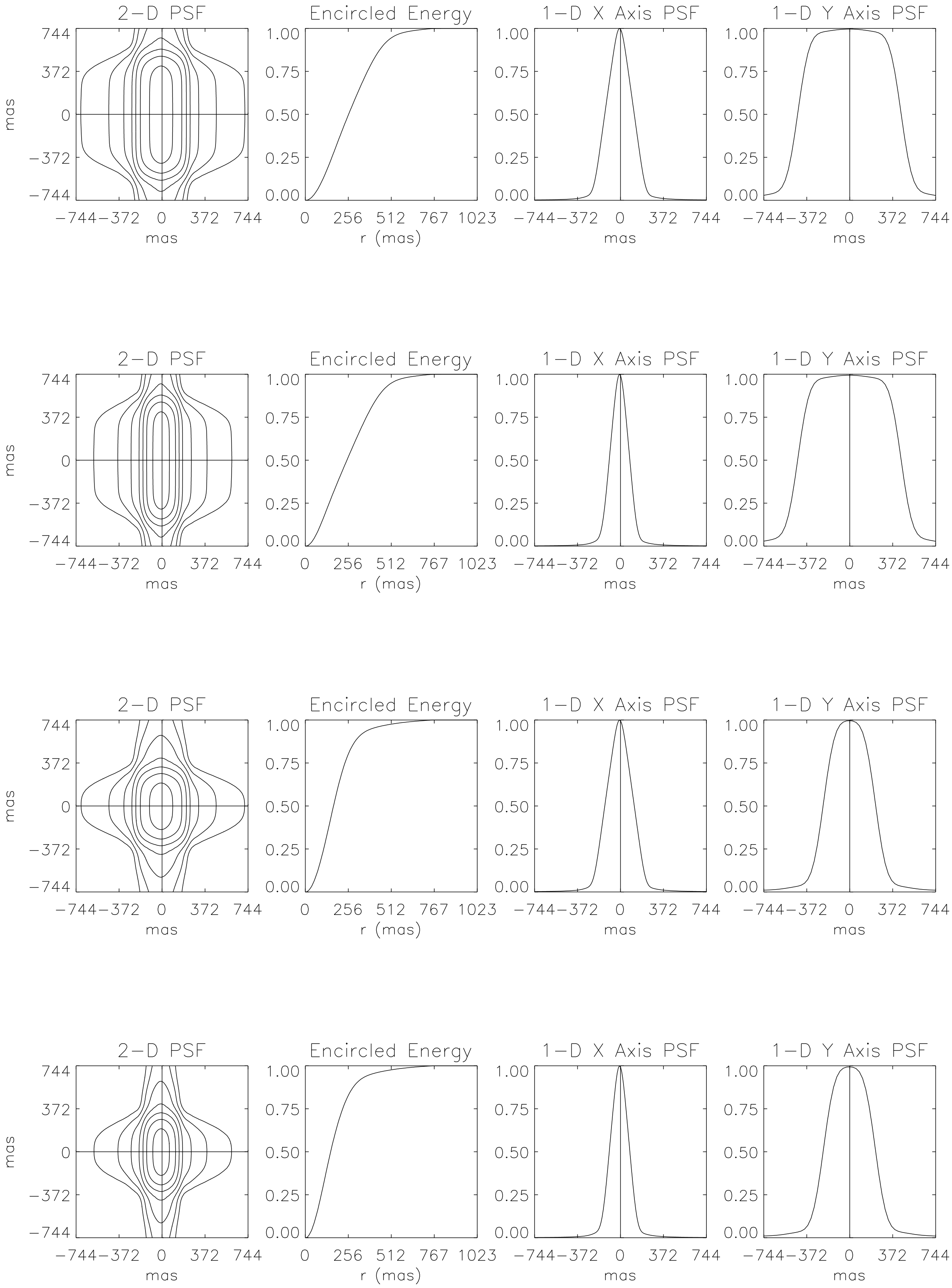

Figure 1: GAIA one-scan PSFs. From the top: (a) 6×8 pixels/sample, (b) 4×8, (c) 6×4, (d) 4×4. See Subsection 3.2 for further explanation.

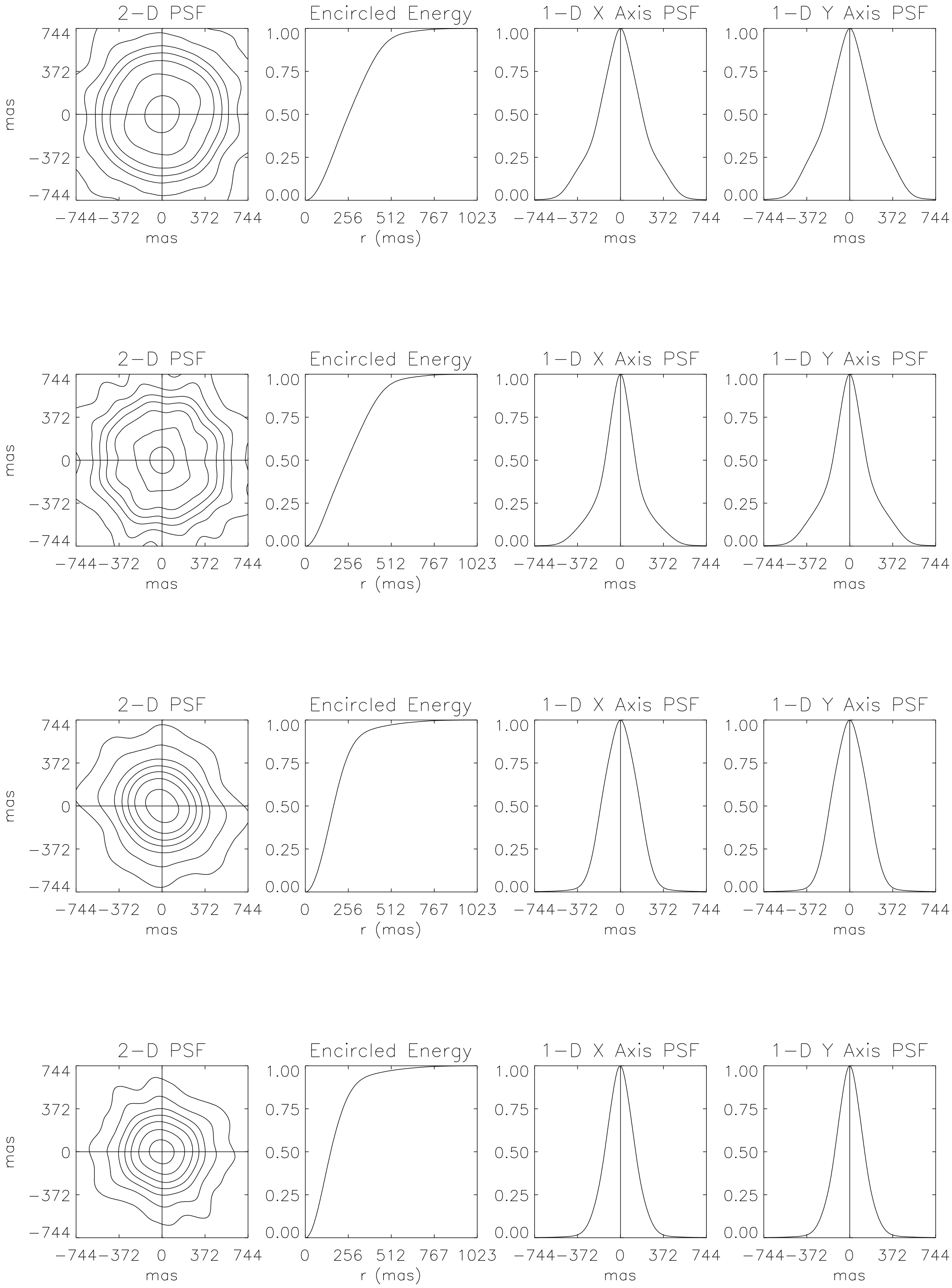

Figure 2: GAIA 50-scan PSFs. From the top: (a) 6×8 pixels/sample, (b) 4×8, (c) 6×4, (d) 4×4. See Subsection 3.2 for further explanation.

The photon noise of the observed signal is usually assumed to follow a Poisson distribution and the relative standard error (i.e. the ratio between the error and the signal) is proportional to $1/\sqrt{N}$, where N is the total number of detected electrons per unit area. Since the exposure times of the WFPC2 images, e.g. 900 s in our case, is much bigger than the integrated GAIA observing times, and since the electron count rate and readnoise of the two instruments are almost the same, it is concluded that for our purposes the photon and readnoise present in the WFPC2 images are negligible.

The readnoise is usually assumed to follow a Gaussian distribution with zero mean and standard deviation independent from the total number of detected electrons. The HST WFPC2 readnoise was measured to be about 5 e^-/pixel rms and 7 e^-/pixel rms, depending on the chosen analog-to-digital conversion gain (see Table 4.3 in Biretta et al. 1996). GAIA readnoise estimation was taken from SAG_CUO_53 (Høg E., Fabricius C., Knude J. and Makarov V.V. 1999) which gives a value of 5.8 e^-/sample rms for a BBP sample of 6×8 pixels and full CCD readout, which is conservative enough since the more recent SAG_MV_04 gives a value of 5.4 e^-/sample rms in the same case.

Note that all the simulations, regardless of the different sample size, were carried out assuming a readnoise of 5.8 e^-/sample rms. Obviously, if full readout of the CCD is needed, a smaller sample size than 6×8 pixels/sample would increase the readnoise, but it is believed this is not required, due to the small size of most galaxies. According to SAG_CUO_61, the half-light radius of a typical galaxy of total I=11 mag is about 25 arcsec, meaning that its half-light circle is well within a diameter of 2 arcmin. The across-scan size of a BBP CCD is 4 arcmin, so that for a galaxy of this magnitude only half the CCD may be readout with 4×8 or 6×4 pixels/sample giving the same reading frequency and therefore the same readnoise as for full CCD readout with 6×8 pixels/sample. Since only some 2000 galaxies out of the 1.5 million we expect to be able to observe are brighter than I=11, most of the time we could even readout the CCD more slowly in order to further reduce readnoise or alternatively further decrease the sample size. For instance, with a sample size of 4×4 pixels/sample we would be able to read an across scan width of about 1.3 arcmin with the same readnoise of 5.8 e^-/sample rms. In so doing, during a single scan we would be able to observe only some parts (e.g. those near the centre of each CCD) of brighter galaxies, which could lead to a low number of total scans for certain sky regions and as a consequence to problems in their stacking, but this could be accepted. Note also that stars and galaxies would be observed by the same instrument, so that in order not to create conflict between the two reading processes the same sample size along scan should be adopted in the two cases.

4 Simulation of Observations

Under our assumptions, the simulation of an observation essentially involves translation and rotation of the original image, scaling and rebinning into samples of its electron counts and smearing due to PSF and noise.

In greater detail, the procedure for the generation of a single simulated observation consists of the following steps:

1. HST counts: HST data number counts are read from the fits file retrieved from the HDA and converted to electron counts using the analog-to-digital conversion gain taken from Table 4.3 in Biretta et al. 1996.

2. Estimation of GAIA counts: GAIA electron counts for a single scan are estimated by taking into account the different exposure time and assuming, according to Subsection 3.1, the same electron count rate for the two instruments.

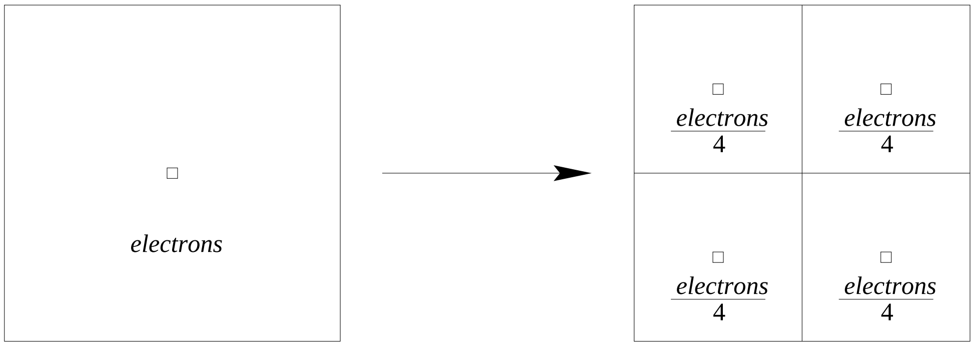

Figure 3: Subdivision of a pixel of the HST image. The central square on the left marks the pixel's centre, whereas the four squares on the right mark the subpixels' centres (cf. Section 4).

3. Subpixeling: in order to improve the resolution of the HST image, each HST pixel is considered as consisting of a mosaic of four square subpixels, "containing" one fourth of the pixel's electrons each and whose centres are displaced from the pixel's centre as shown in Figure 3.

4. Subpixels' translation and rotation: since the observation will in general have a different orientation and a different centre with respect to the original image, the subpixels are translated and rotated accordingly to the desired observation's scan direction and centre.

5. Rebinning of GAIA observation: each subpixel electron count is assigned to the sample containing its centre.

6. Convolution with GAIA PSF: the observation is finally convolved with the PSF described in Section 3.2.

7. Noise addition: to simulate photon noise we calculated a Poisson deviate of the observation, whereas to simulate readnoise we added to it a Gaussian distribution with zero mean and standard deviation equal to the rms readnoise.

When generating a realistic all-mission set of n_{obs} simulated observations, however, one has to take into account that in general the observations of a given sky region will have different scan directions as well as different centres. Therefore, a set of n_{obs} randomly distributed scan directions (in the range from 0^o to 360^o) and observations' centres' coordinates along both axes (in the range from $-samsize/2$ to $samsize/2$, where $samsize$ is the adopted sample size along one of the two axes) is generated (Note that the consequences of possible preferred scan directions are described in Section 6). Then the procedure described above can then be applied to each observation.

5 Stacking of Observations

The stacking of a single simulated observation into a flux map involves the following steps:

1. Subsampling: to recover some of the resolution lost in the sampling process each sample is considered as consisting of a mosaic of square subsamples of 37.2 mas side, each containing the same fraction of the sample electron count, much like it is done in Section 4 and shown in Figure 3 for the subpixeling. The value of 37.2 mas, i.e. the CCD pixel size in the along

scan direction, was chosen so as to be smaller than the side of the flux map elements and to be an integer submultiple of the sample size along both directions, so that each sample can be divided into an integer number of subsamples.

2. Subsamples' translation and rotation: the mosaic of subsamples is counter-translated and counter-rotated to superpose it onto the flux map, which is a mosaic of 50 mas step having the same orientation and the same centre as the original image.

3. Rebinning of GAIA flux map: each subsample electron count is assigned to the flux map element containing its centre.

This procedure returns a one-scan flux map. The all-mission flux map is then simply obtained by adding up all the one-scan flux maps from observations of a given sky region.

6 Flux Maps of M100

As an example, we present simulations based on a PC image of the spiral galaxy M100. This was chosen because it contained many of the interesting features one would like to observe in galaxies; a bright core, sharp surface brightness variations, spiral arms and HII regions. The central part of this image, namely a square of about 16 arcsec side whose flux map was reconstructed from the simulated observations, is shown in Figure 4. For this galaxy the RC3 (de Vaucouleurs et al. 1991) reports a total V magnitude of 9.35 and an half-light radius of about 104 arcsec, meaning that the PC image, with a side of 36.4 arcsec, covers its very central parts only. The median surface brightness in V inside the eight zones marked by letters is given in Table 2. The position of five bright HII regions, which in Section 7 will be used to roughly assess the photometric accuracy achievable by the flux maps, is marked by numbers. Note that the median surface brightness of the whole image is $\mu_V = 19.42$ mag/arcsec^2.

Table 2: Characteristic values of surface brightness in V of the HST image. Median surface brightness in V inside zones of diameter 1.0 arcsec indicated in Figure 4.

	median μ_V mag/arcsec^2
a	19.10
b	20.65
c	20.71
d	18.96
e	17.83
f	18.35
g	17.59
h	16.80

In the flux maps generation, a conservative number of 50 scans, i.e. an effective exposure time of 45 s, was assumed. Note that this is the minimum number of times an Astro Instrument would scan any sky region during a 5-year mission, according to Figure 2 in SAG_LL_26 (Lindegren 1999b).

The flux maps obtained for different sample sizes by stacking of 50 simulated observations are displayed in Figure 5, showing that among the considered sizes, a smaller sample size gives a better resolution. It also appears that flux maps obtained with bigger sample sizes are fairly smooth whereas those obtained with smaller sample sizes show a conspicuous lumpiness, but

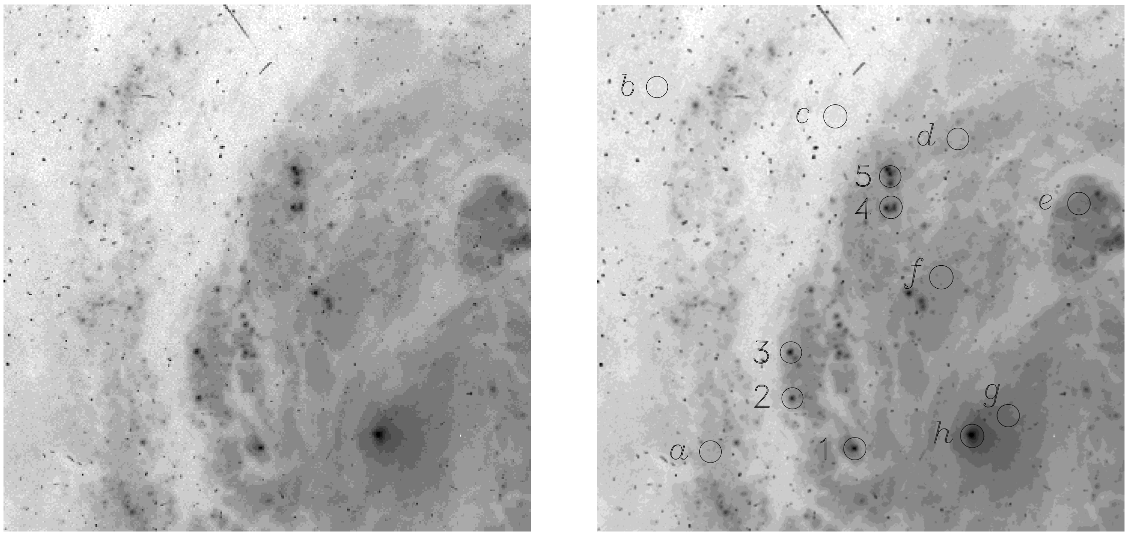

Figure 4: HST image. WFPC2 PC image of the spiral galaxy M100, obtained with a 900 s exposure with the F555W filter, similar to V. The image side is about 16 arcsec and the circles have a diameter of about 0.7 arcsec. (a–h): position of the eight zones of diameter 1.0 arcsec used to calculate the median surface brightness in Table 2. (1–5): five HII regions of which aperture photometry is carried out in Section 7.

this is well understood as produced by features in the HST image, viz. faint stars but mostly cosmic ray hits, which otherwise could not be seen due to a wider PSF.

However, the flux maps resolution obtainable with different sample sizes is better illustrated by Figure 6, showing two HII regions near the centre of the flux maps with a separation of about 0.5 arcsec. It appears that an overall resolution of about 350 mas would be obtained with 6×4 pixels/sample, which is the only sample size considered in the following, corresponding to an image obtained with an excellent large ground-based telescope during the short times of superb seeing. The best image obtained by the VLT had just about this small stellar image size. Note that this choice would allow to maintain the baseline sample size of 6×8 pixels for the observation of stars, since the size along scan would be the same in the two cases.

The resolution improvement due to the increase in the number of scans can be seen in Figure 7, showing the same part of the flux map as in Figure 6 as it is seen in a single observation with 6×4 pixels/sample and as it is reconstructed from 10 simulated observations with the same sample size. The latter image shows that the highest resolution allowed by GAIA PSF could be achieved with a number of scans substantially smaller than the 50 presently assumed.

An important issue is also how a non-random set of scan directions, where some angles appear much more frequently than others, could affect the resolution of the flux maps. Actually, since the samples we considered are rectangular and with the major side perpendicular to the scan direction, the presence of a preferred scan direction in principle implies a loss of resolution, due to the PSF elongation, perpendicularly to this direction. Obviously the problem increases with the PSF asymmetry, and Figure 8 shows that for a sample size of 6×4 pixels its effects are negligible in the case of scan directions all concentrated in an interval of 90°, but not so when the interval is reduced to 45°. The latter case is however an extreme one, which is not likely to occur in practice.

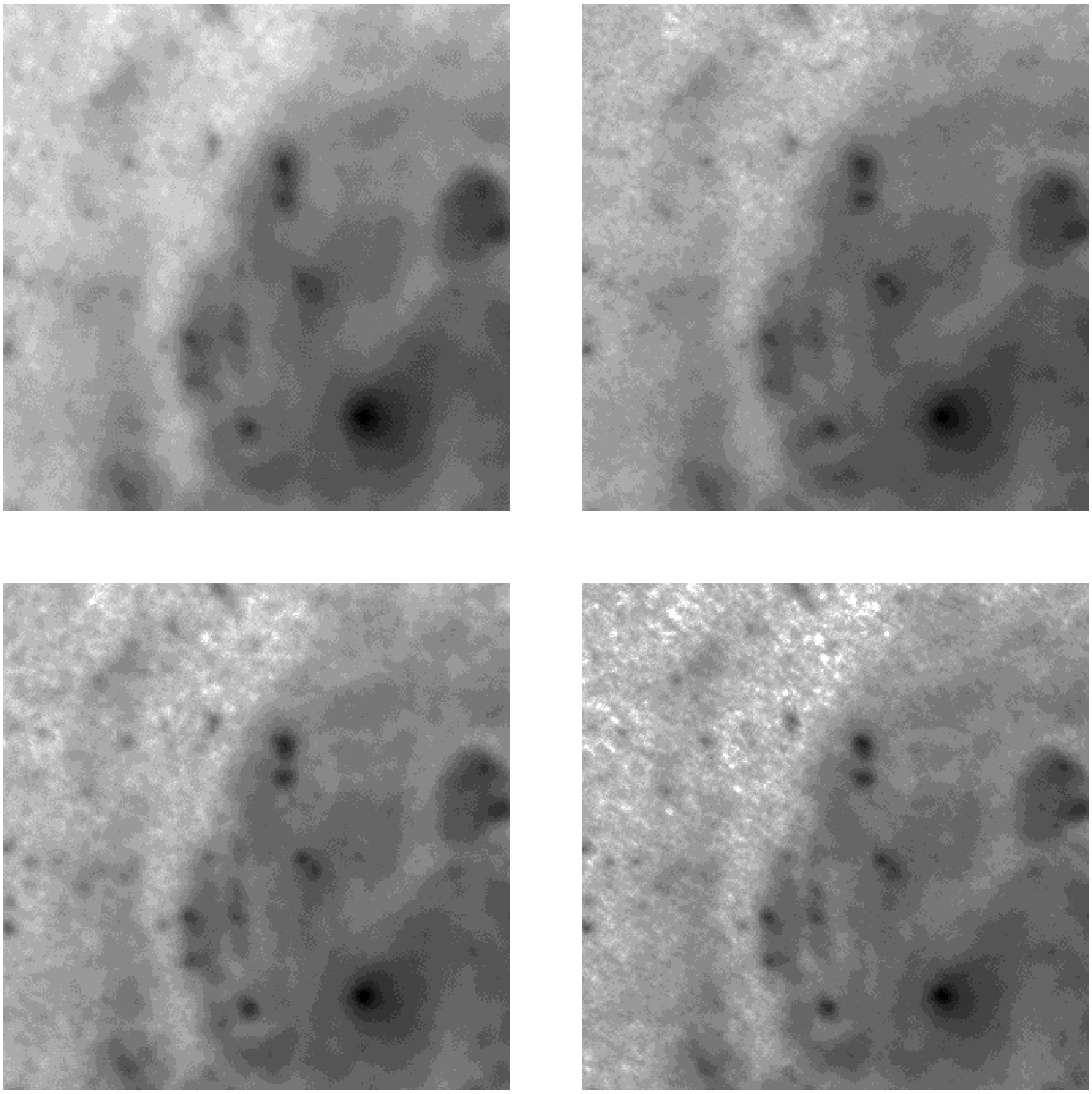

Figure 5: GAIA flux maps. BBP flux maps reconstructed from 50 simulated observations in V, i.e. with an effective exposure time of 45 s, for different sample sizes. Upper row: 6×8 and 4×8 pixels/sample. Lower row: 6×4 and 4×4. The side of each flux map is 16 arcsec. The lower row shows the better resolution. This is accompanied by a lumpy structure of the faint parts of the background due to faint stars and (mostly) cosmic ray hits in the HST image.

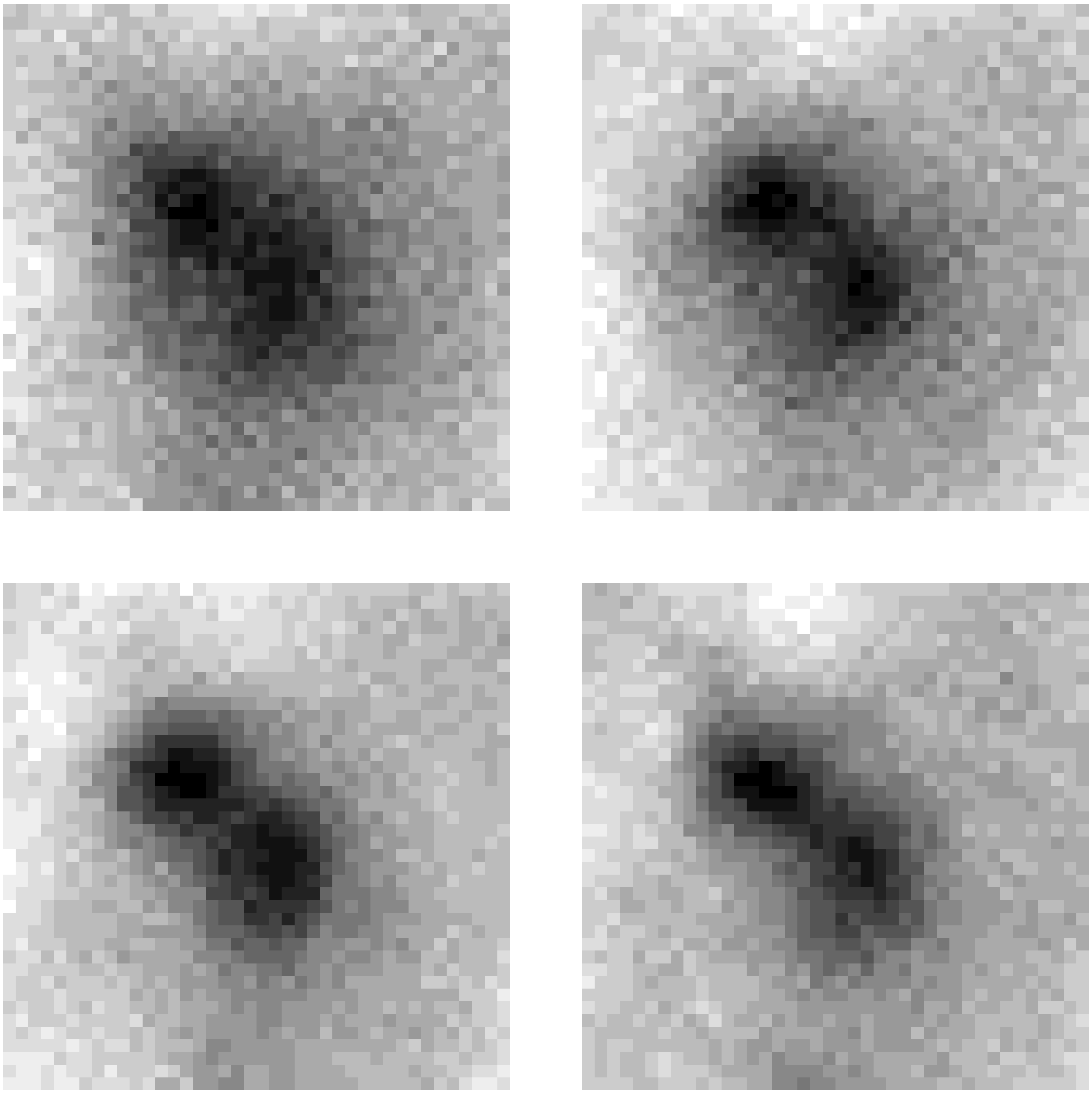

Figure 6: A part near the centre of GAIA flux maps in Figure 5. Upper row: 6×8 and 4×8 pixels/sample. Lower row: 6×4 and 4×4. Two HII regions with a separation of about 0.5 arcsec are clearly better resolved with 6×4 pixels/sample than with 6×8 or 4×8 while a further decrease in the sample size to 4×4 does not give significant improvement. The side of each image is 2 arcsec.

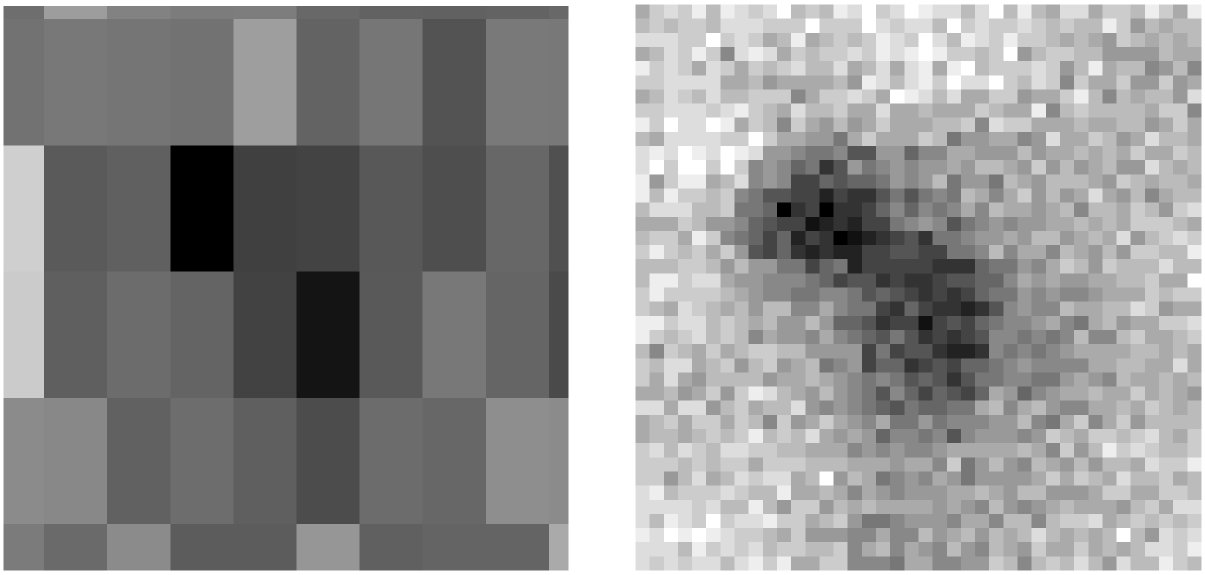

Figure 7: Number of scans and resolution of flux maps. The two images show the same sky region of 2×2 arcesc^2 as in Figure 6. The left image shows a single observation obtained with 6×4 pixels/sample and the right image shows a flux map reconstructed from 10 simulated observations with the same sample size.

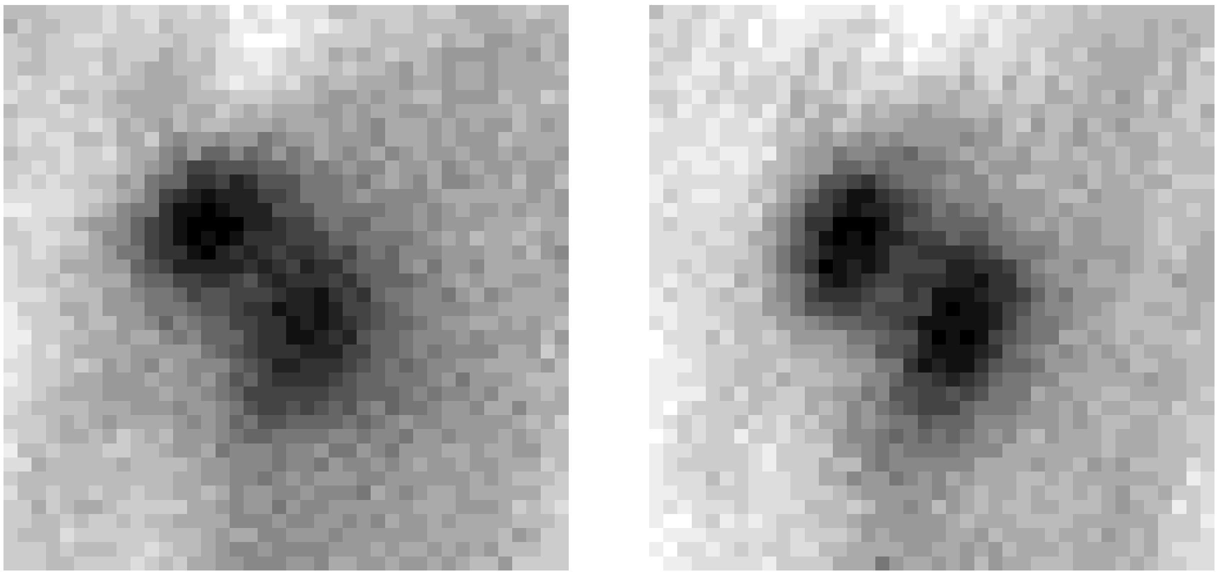

Figure 8: Non-random scan directions and resolution of flux maps. The two images show the same sky region of 2×2 arcsec^2 as in Figures 6 and 7, but the flux maps are here reconstructed from 50 simulated observations with non-random scan directions. The sample size is 6×4 pixels and the scan directions are concentrated in an interval of 90^o and 45^o for the left and right image, respectively. In the former case the image distortion is negligible compared to Figure 6c. In the latter case the two HII regions show an increased elongation.

7 Photometry of Flux Maps

As a verification of the simulation procedure, and to roughly estimate the photometric accuracy obtainable from the analysis of the flux maps, aperture photometry of the five HII regions shown in Figure 4 was carried out. The HDA calibrated data and the flux map data obtained by stacking of 50 simulated observations with 6×4 pixels/sample were separately used. The centre of the HII regions was determined by visual inspection, the signal counts inside a radius of 500 mas were summed and a median background calculated inside an annulus of radii 500 mas and 2000 mas was subtracted.

The results are given in Table 3. In order to take into account the different exposure time of the two images, the electron counts obtained from GAIA flux maps were multiplied by 20, i.e. the ratio between the exposure time of the HST original image (900 s) and the effective exposure time of a flux map reconstructed from 50 observations (45 s). The second column gives the HST electron counts corrected for the background, the third one gives GAIA electron counts corrected for the background and scaled to the HST exposure time, the fourth one gives the bias in magnitudes of the flux map with respect to the HST data and the fifth one gives the Landolt V magnitude of the HII region according to the WFPC2 photometric calibration obtained by Holtzman et al. 1995b, adopting a colour index of $V - I = 1.0$.

A bias of about 0.2 mag towards faint magnitudes is clearly seen, together with a standard error of the result from 50 observations of about 0.05 mag, estimated from the agreement between the five values in the fourth column. A more careful inspection of the data shows that this bias is due to an underestimation of the signal counts of about 0.1 mag as well as to an overestimation of the background of about 0.3 mag. Both biases are easily understood as due to the wide wings of the GAIA PSF, which cause some energy to fall out of the 500 mas radius and thus in the outer annulus. A smaller contribution to the systematic error affecting the background determination seems to originate from the smearing of almost point-like features like faint stars and cosmic ray hits present in the HST image. Their smearing cause their electron counts, which as far as possible should not be considered in the background calculation, to spread over a fairly large area and thus to "escape" the median method used to reject them in the calculation of the background. Note also that the bias in aperture photometry described above depends strongly on the sample size, being of about 0.5 mag with random fluctuations at the level of 0.1 mag for flux map obtained with 6×8 pixels/sample.

Table 3: Aperture photometry of five HII regions. HST electron counts, GAIA electron counts scaled to the HST exposure time, bias in magnitudes and Landolt V magnitude of the HII regions in the HST image. A flux map obtained from 50 observations with 6×4 pixels/sample was used. The position of the HII regions on the HST image is given in Figure 4b.

HII region	E_{HST}	$20\,\mathrm{E}_{GAIA}$	$\frac{20\,\mathrm{E}_{GAIA} - \mathrm{E}_{HST}}{\mathrm{E}_{HST}}$	V_{HST}
	e^-	e^-	mag	mag
1	192769	159549	-0.172	18.8492
2	147170	115019	-0.218	19.1423
3	178634	137214	-0.232	18.9319
4	222181	198978	-0.104	18.6950
5	361727	304130	-0.159	18.1659

8 Conclusions

Simulated observations of galaxies with GAIA BBP and their stacking into flux maps were presented, based on HST WFPC2 images and on realistic assumptions about GAIA performance.

The issue of determining the optimal sample size for these observations was addressed by comparing flux maps obtained with four different sample sizes. It is concluded that with respect to the baseline size of 6×8 pixels foreseen for the Astro-2 the choice of a smaller size of 6×4 pixels yields both higher resolution and more accurate photometry of the flux maps. This is not in conflict with the use of the baseline sample size for the observation of stars. With a sample size of 6×4 pixels and a conservative number of 50 scans, the flux maps would have a resolution of about 350 mas. Under the same assumptions, the aperture photometry in V of an HII region of $V \simeq 18$–19 mag would probably have a bias of 0.2 mag, which could at least partly be corrected, and a standard error of about 0.05 mag, which depends on the background level and structure. The only drawback of adopting a smaller sample size is the higher reading frequency (and thus readnoise/sample) that would be needed for full CCD readout, but this could be coped with by reading only a part of the CCD, which is actually sufficient for most galaxies. Accordingly, all the simulations were carried out assuming the same readnoise/sample foreseen for 6×8 pixels/sample and full CCD readout. The photometric results could undoubtedly be improved, especially by application of PSF photometry instead of aperture photometry, but this was beyond the scope of the present study.

These results demonstrate the feasibility of galaxy observations and the advantage to observe with 6×4 pixels/sample in the Astro-2 instrument when a galaxy is detected.

References

[1] Biretta J.A. et al. 1996, WFPC2 Instrument Handbook, Version 4.0, Baltimore STScI

[2] de Vaucouleurs G. et al. 1991, Third Reference Catalogue of Bright Galaxies, University of Texas Press

[3] Høg E., Fabricius C., Knude J. and Makarov V.V. 1999, Sky survey and photometry by the GAIA satellite, Technical Report SAG_CUO_53

[4] Holtzman J. et al. 1995a, PASP, 107, 156

[5] Holtzman J. et al. 1995b, PASP, 107, 1065

[6] Lindegren L. 1999a, Point Spread Functions for GAIA including aberrations, Technical Report SAG_LL_25

[7] Lindegren L. 1999b, Simulation of GAIA scanning of arbitrary directions, Technical Report SAG_LL_26

[8] Vaccari M. and Høg E. 1999, Statistical model of galaxies, Technical Report SAG_CUO_61

[9] Vaccari M., Høg E. and Makarov V.V. 1999, Three images of M100, Technical Report SAG_CUO_66

[10] Vannier M., Noise of GAIA Astro Instrument, Technical Report SAG_MV_04